J. Fluid Mech. (2000), *vol.* 405, *pp.* 305–323. Printed in the United Kingdom

Transitions of flow past a row of square bars

By J. MIZUSHIMA AND Y. KAWAGUCHI

Department of Mechanical Engineering, Doshisha University, Kyotanabe, Kyoto 610-0321, Japan

(Received 19 January 1999 and in revised form 28 October 1999)

Transitions of flow past a row of square bars placed across a uniform flow are investigated by numerical simulations and the bifurcation analysis of the numerical results. The flow is assumed two-dimensional and incompressible. It is already known that jets coming through gaps between square bars are independent of each other when the pitch-to-side-length ratio of the row is large, whereas the confluence of two or three jets occurs due to a first pitchfork bifurcation from the flow with independent jets when the pitch-to-side-length ratio is small. It is found that confluence of four jets occurs in consequence of the second pitchfork bifurcation from the flow with pairs of jets joined to each other. Bifurcation diagrams of the flow are obtained, which include confluences of double, triple and quadruple jets. Lengths of the twin vortices are evaluated for each flow pattern. The confluences of two, three and four jets are qualitatively confirmed experimentally by flow visualizations.

1. Introduction

Wakes behind a row of bars have been studied extensively by many experimentalists who work with wind tunnels, where they use a narrow spaced row of bars to obtain a uniform velocity distribution without large-scale fluid motions. However, the narrow spaced row of bars often induces large-scale vortices and prevents the velocity distribution from becoming uniform when the bars are put too close to each other. This is due to the confluences of several jets coming through the gaps between bars.

Bohl (1940) did experiments on several rows of parallel polygonal bars and observed the combining of jets when the pitch-to-diameter ratio σ is smaller than about 2.2, where σ is the ratio of the spacing P to the diameter d of the bars. Experimental results by Bradshaw (1965) suggest that the critical value of σ is about 2.3, above which the combining of jets does not occur in the range of Reynolds number typical of wind tunnel practice. The Reynolds number dependence of the phenomena was investigated by Matsui (1975). He did detailed experiments on a row of circular bars and observed parallel jets at $\sigma = 3.0$, and combining of two, three and four jets at $\sigma = 2.2$, 1.8 and 1.6 respectively at $Re = 2000$, where the Reynolds number is defined as $Re = Ud/\nu$, U being the upstream velocity, d the diameter of the circular bars and ν the kinematic viscosity of the fluid. Moretti & Chen (1987) re-examined the instability of the flow by experiments and concluded that a more complex instability occurs for $\sigma \leqslant 1.5$. A brief review of experiments on the flow past a row of bars is given by Moretti (1993).

Most experiments so far have been performed at $Re \sim 10^3$, where the wakes are more or less turbulent. However, it was also found that mutual interactions of jets lead to a time-periodic flow where detached vortices from bars make a periodic

pattern with double the period of the bars in the normal direction to the flow at smaller Reynolds numbers ($Re \sim 210$) (see Kobayashi 1984). At still smaller Reynolds numbers ($Re \sim 20$–50), the phenomenon of the confluence of two, three or four jets was found in steady wakes (Mizushima & Takemoto 1996).

The confluence phenomenon has been attributed to the 'Coanda effect' by many researchers as described in the review by Moretti (1993). The Coanda effect is assigned when a jet-like stream tends to attach to a rigid boundary or to bend along a boundary surface, but it does not explain any breaking of the symmetry or any change of periodicity in the flow field past a row of bars. It had been expected that bifurcation or stability theory may give physical insight into the underlying mechanism of the phenomena.

Theoretical attempts to clarify the mechanism of the confluence of jets were made by Gotoh, Yamada, & Mizushima (1983), Green (1974) and Beaumont (1981). They assumed a parallel flow that is periodic in the direction normal to the stream as the basic flow and did a linear stability analysis. However, the critical mode of disturbance was found to have the same period as the basic flow and the mechanism of the confluence of jets could not be successfully explained in spite of an extension to a weakly nonlinear stability analysis (Yamada 1986).

A comprehensive explanation of the confluence of two or three jets in steady wakes was given by Mizushima & Takemoto (1996) (hereafter referred to as MT). They did numerical simulations and analysed the numerical results by using bifurcation theory. It was shown that the confluence of two or three jets occurs due to a pitchfork bifurcation from the flow with parallel jets. In other words, the flow with parallel jets becomes unstable at a critical Reynolds number when the Reynolds number is increased, and another flow with two or three jets combined appears as a consequence of the instability above the critical Reynolds number. They evaluated the critical Reynolds numbers Re_{c2} and Re_{c3} where the confluence of two or three jets occurs in the range $\sigma = 1.6$–2.5. Their theoretical results were confirmed by their own experiments, but there was a discrepancy between the values of Re_{c3} obtained by numerical simulations and experiments. They conjectured that the discrepancy may be due to hysteresis phenomena caused by instabilities of the nonlinear solutions of the flows with two or three jets combining.

The present paper is an extension of MT. We investigate the transitions of flow past a row of square bars placed across a uniform flow by numerical simulations and the bifurcation analysis of the numerical data. The flow is assumed two-dimensional and incompressible. We focus our attention to the mechanism of the confluence of four jets. We also evaluate the lengths of the twin vortices for each flow where jets are parallel, or two, three, four jets combined and obtain the pressure distribution for each flow, which was absent in MT. The confluence phenomenon of jets is confirmed experimentally by flow visualizations.

2. Method of numerical simulation

We assume a two-dimensional and incompressible flow field; then the governing equations, the equation of continuity and the Navier–Stokes equation are written in dimensionless forms as

$$\nabla \cdot \boldsymbol{u} = 0, \tag{2.1}$$

$$\frac{\partial \boldsymbol{u}}{\partial t} + (\boldsymbol{u} \cdot \nabla)\boldsymbol{u} = -\nabla p + \frac{1}{Re}\nabla^2 \boldsymbol{u}, \tag{2.2}$$

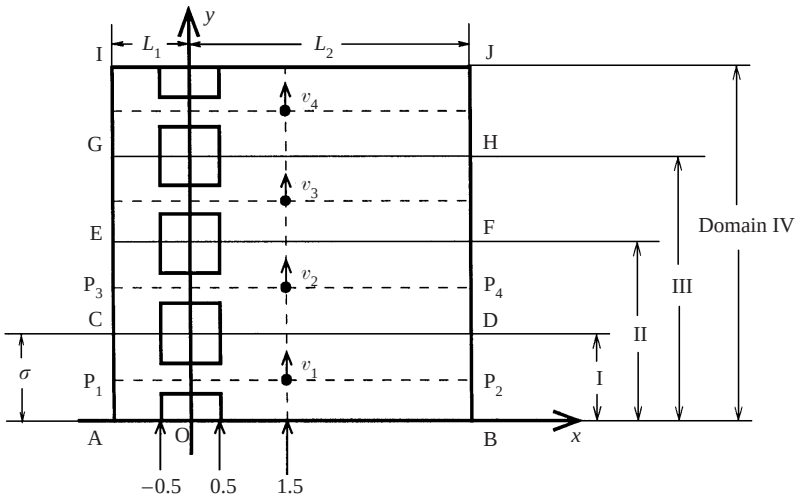

FIGURE 1. Coordinates and computational domains. ABDC: Domain I, ABFE: Domain II, ABHG: Domain III, ABJI: Domain IV.

where the Reynolds number Re is defined as $Re \equiv Ud/v$, U being the uniform upstream velocity, d the side length of the square bars and v the kinematic viscosity, and all the variables are normalized by using the representative velocity U and length d. We use the primitive variables $\boldsymbol{u} = (u, v)$ and p for numerical simulations. In conventional numerical simulations, initial value problems are solved under a certain boundary condition for a given set of values of parameters (σ, Re), where only stable solutions are obtained as steady solutions. Our strategy here is to attempt to calculate all the steady solutions regardless of their stability by imposing appropriate boundary and symmetry conditions on each steady solution, although it is not always possible to obtain all the steady solutions as described later. We focus our attention on the change in the number of steady solutions and evaluate the critical values of the parameters at which the number of solutions changes. We do not study the linear stability of the steady solutions here, but some partial knowledge about the stability can be obtained from the numerical results calculated under various boundary and symmetry conditions.

2.1. *Computational domain and the boundary conditions*

We restrict ourselves to flows with each jet independent and two, three, or four jets combining, and call them σ-flow, 2σ-flow, 3σ-flow and 4σ-flow respectively. In order to calculate all the steady solutions, we impose corresponding boundary and symmetry conditions on each solution. We define four computational, domains I, II, III, IV, which have widths σ, 2σ, 3σ, 4σ in the direction normal to the stream as shown in figure 1. Flows are assumed periodic in that direction in each domain. We impose a symmetry condition on each flow field along the centreline of each domain, so that actual computational regions are reduced to a half of each domain. Note that these restrictions may exclude other solutions without periodic and symmetry conditions, but do not set arbitrary limits on the range of symmetric and asymmetric solutions.

We take the Cartesian coordinates as shown in figure 1, where the origin is taken at the centre of one of the bars, the x-axis parallel to the upstream uniform flow and the y-axis perpendicular to it. The x- and y-coordinates are normalized by the side length d of the square bar in this figure. The length of the domain in the streamwise

direction is $L_1 + L_2$, where L_1 is the upstream length and L_2 the downstream length from the origin. The lengths L_1 and L_2 are taken large enough not to affect the numerical results. We adopt $L_1 = 4.5$ and $L_2 = 10.5$ in all our numerical simulations except for domain IV where larger length $L_2 = 11.5$ is adopted.

The numerical solution for the steady flow with four jets combining, i.e. 4σ-flow, can be calculated in the domain ABJI, i.e. domain IV, in figure 1. We will explain the boundary and symmetry conditions by adopting domain IV as an example. Flow fields are assumed periodic with the period 4σ in the y-direction and symmetric along the line AB and EF in domain IV, so that the computational domain can be reduced to a half of ABJI, i.e. ABFE. Assuming a uniform flow on AE, the boundary conditions of the velocity and the pressure are written as

$$u = 1, \quad v = 0, \quad \frac{\partial p}{\partial x} = 0 \quad \text{at } x = -L_1. \tag{2.3}$$

For an outflow boundary condition on BF, we use boundary conditions that the streamwise derivatives of the velocity and the pressure are zero, i.e.

$$\frac{\partial u}{\partial x} = 0, \quad \frac{\partial v}{\partial x} = 0, \quad p = 0 \quad \text{at } x = L_2. \tag{2.4}$$

We utilize the symmetric conditions $v(x,0) = 0$, $\partial u(x,0)/\partial y = 0$ and $\partial p(x,0)/\partial y = 0$ on EF and AB, which are expressed as

$$u(x,y) = u(x,-y), \quad v(x,y) = -v(x,-y), \quad p(x,y) = p(x,-y) \quad \text{on AB}, \tag{2.5}$$

$$\left.\begin{array}{l} u(x,2\sigma - y) = u(x,y - 2\sigma), \quad v(x,2\sigma - y) = -v(x,y - 2\sigma), \\ p(x,2\sigma - y) = p(x,y - 2\sigma) \quad \text{on EF}. \end{array}\right\} \tag{2.6}$$

On the surfaces of the square bars, non-slip boundary conditions are applied as follows:

$$u = 0, \quad v = 0. \tag{2.7}$$

Under the boundary and symmetry conditions (2.3)–(2.7) in domain IV, steady solutions attainable by our numerical simulations are σ-flow, 2σ-flow and 4σ-flow. Only 3σ- and σ-flows can be obtained in domain III, whereas σ- and 2σ-flows are possible in domain II; only σ-flow is attainable in domain I.

2.2. *Finite difference approximation*

We use the MAC method with a staggered mesh. The MAC method is very popular and it is briefly summarized here. The basic equations are the equation of continuity (2.1), and the Navier–Stokes equation (2.2), which are written in terms of primitive variables. Following the MAC method, the Poisson equation for the pressure p is derived by taking divergence of (2.2) as

$$\nabla^2 p = -\nabla \cdot \{(\boldsymbol{u} \cdot \nabla)\boldsymbol{u}\} + \frac{1}{Re}\nabla^2 D - \frac{\partial D}{\partial t}, \tag{2.8}$$

where $D \equiv \nabla \cdot \boldsymbol{u}$. Although the second and the third terms are identically zero due to the continuity (2.1), they are retained as correction terms in order to prevent the accumulation of numerical errors. If $\boldsymbol{u}$ is given at a certain time, p can be calculated from the Poisson equation (2.8). Then by substituting these values into (2.2), the velocity $\boldsymbol{u}$ at the next time is calculated from (2.2).

The computational domain is discretized by equally distributed increments Δx, Δy in the x- and y-directions. The mesh points are indicated by indices i and j which

	Δx	Δy	v_1
Present study (equal mesh)	0.1	0.025	0.208
	0.05	0.025	0.197
	0.025	0.025	0.196
MT (unequal mesh)	0.1	$0.02 \sim 0.1$	0.207

TABLE 1. Values of $v_1 \equiv v(1.5, \sigma/2)$ for three different sets of mesh sizes, and comparison of our results with those by MT. $Re = 40$, $\sigma = 2.0$.

count along the x- and y-directions respectively. The time t is also discretized by Δt and is indicated by an index n. Then the velocity $\boldsymbol{u} = (u, v)$ and the pressure p are expressed as $u(x, y, t) = u(i\Delta x, j\Delta y, n\Delta t) = u_{ij}^n$, $v(x, y, t) = v(i\Delta x, j\Delta y, n\Delta t) = v_{ij}^n$ and $p(x, y, t) = p(i\Delta x, j\Delta y, n\Delta t) = p_{ij}^n$. The magnitudes of Δx, Δy and Δt are taken as $\Delta x = 0.05$, $\Delta y = 0.025$ and $\Delta t = 0.003$ in our numerical simulations. The number of mesh points is 300×80 for the case of the $\sigma = 2.0$ in domain II, for instance.

In (2.2), the time and the pressure derivatives are approximated by the first-order forward difference, and other terms in (2.2) and all the terms in (2.8) are approximated by the second-order central difference. Equation (2.8) for p_{ij}^n is solved by the SOR iterative method. The convergence of the iteration is judged by the criterion $\max_{ij} |(p_{ij}^n)^k - (p_{ij}^n)^{k-1}| < 10^{-7}$, where k denotes the number of iteration cycles. The flow field is judged to attain its steady state if $\max_{ij} |\boldsymbol{u}_{ij}^{n+1} - \boldsymbol{u}_{ij}^n| < 5.0 \times 10^{-7}$.

2.3. *The accuracy of numerical simulations*

The accuracy of numerical simulations is confirmed by comparing our results with those by MT. We adopt the velocity v_1 in the y-direction at $(x, y) = (1.5, \sigma/2)$ for the case of 2σ-flow as a representative quantity. The lengths $L_1 = 4.5$ and $L_2 = 10.5$ are taken as the same values as MT, who solved the same problem numerically by using the MAC method with a non-staggered and non-equally distributed mesh, and also by ψ–ω method. It is noted that the boundary conditions for the pressure p are different between our numerical method and theirs. We take boundary conditions (2.3) and (2.4) although they fixed $p = 0$ at $x = -L_1$ and $\partial p/\partial x = 0$ at $x = L_2$. Our boundary conditions (2.3) and (2.4) are considered better for numerical stability for MAC method with a staggered mesh.

We tabulate the values of v_1 obtained by our numerical simulation with $\Delta x = 0.1$ and $\Delta y = 0.025$ in table 1, where the results of MT are also listed for comparison. The difference between our results and those by MT is 0.5% at most. We also compare the values of v_1 for two different sets of mesh sizes $(\Delta x, \Delta y) = (0.05, 0.025)$ and (0.025, 0.025). The relative error of v_1 between the two cases is 0.5% at most. So, we decided that the discretization sizes $(\Delta x, \Delta y) = (0.05, 0.025)$ are small enough, and we use that throughout this paper.

3. Numerical results

The confluence of two or three jets in the flow past a row of square bars was found by numerical simulations of MT and confirmed experimentally by them, where the mechanism of the confluence was clarified as being due to pitchfork bifurcations. They evaluated the critical Reynolds numbers Re_{c2} and Re_{c3} at which σ-flow bifurcates to 2σ-flow or 3σ-flow in the range of $1.6 \leqslant \sigma \leqslant 2.5$. We reconfirm their results and evaluate the values of Re_{c2} and Re_{c3} in the range of $1.4 \leqslant \sigma \leqslant 1.7$, then clarify the

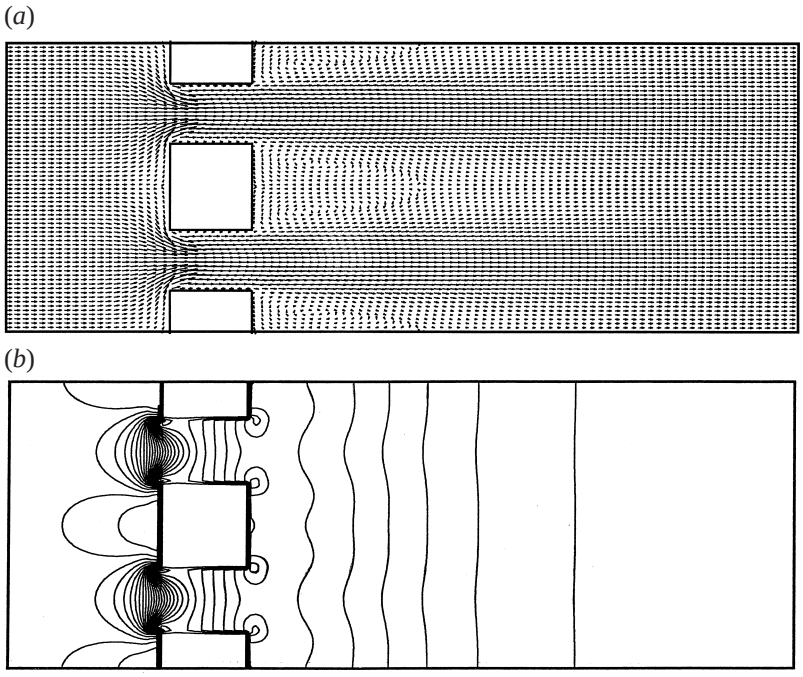

FIGURE 2. Flow fields. $Re = 24.0$, $\sigma = 1.7$. (*a*) Velocity field (velocity vectors). Stable σ-flow. Domains I, II, III, IV. (*b*) Pressure (isobars). Stable σ-flow. Domains I, II, III, IV.

mechanism of the confluence of four jets and evaluate the critical Reynolds number Re_{c4} at which 4σ-flow appears.

3.1. *Flow fields and bifurcations*

We have done numerical simulations in all the four domains I–IV for various values of the Reynolds number, where several initial conditions are adopted. One typical initial condition is a uniform flow except for the boundary of the bars and another is the steady flow obtained for a nearby Reynolds number. We will show four flow fields at $Re = 24$, 26, 27.5 and 30 for the case of $\sigma = 1.7$ as typical flow patterns and discuss the transition of the flow.

We can obtain only one steady flow solution in all the four domains I–IV for small values of the Reynolds number even if we repeat the numerical simulations by adopting various different initial conditions. The steady flow pattern at $Re = 24$ is depicted in figure 2(*a*), where velocity vectors at mesh points used in the numerical simulations are shown by arrows in domain II. In figure 2(*a*), we can see that jets coming through gaps between square bars are independent of each other and the flow field has a periodicity of σ in the y-direction. The corresponding pressure field is shown in figure 2(*b*), where the pressure distribution is drawn by contour lines. We can see a high pressure gradient at the entrance to the narrow gaps between the bars. The pressure approaches a constant value $p = 0$ far downstream.

We can obtain 2σ-flow at $Re = 26$ in domains II and IV as shown in figure 3(*a*). The confluence of two jets is seen from the pressure field in figure 3(*b*) as well as the velocity field in figure 3(*a*). The twin vortices attached to the bars have two different lengths that alternate as shown in figure 3(*a*): the twin vortices attached to the bars at the top and bottom are larger than those attached to the middle bar. We

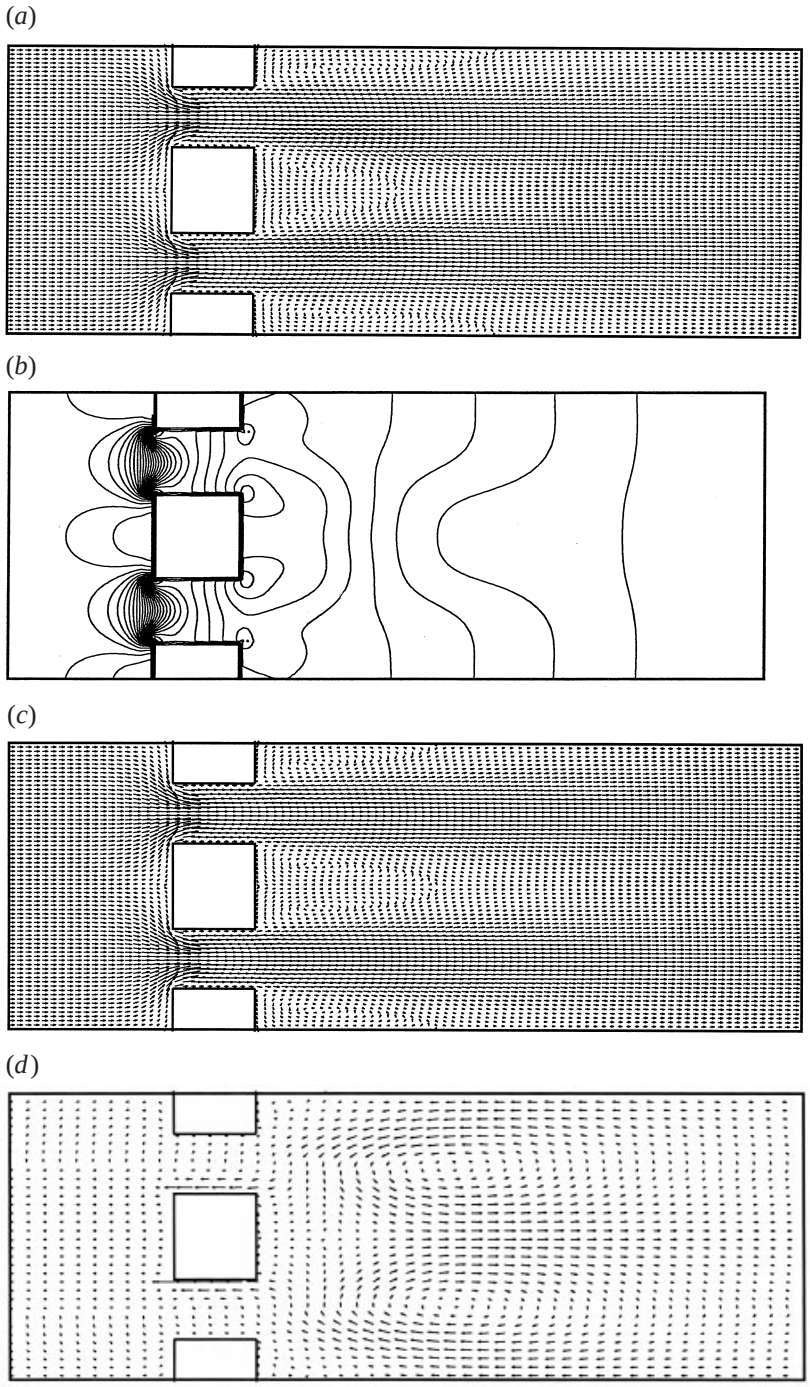

FIGURE 3. Flow fields. $Re = 26.0$, $\sigma = 1.7$. (*a*) Velocity field (velocity vectors). Stable 2σ-flow. Domains II, IV. (*b*) Pressure (isobars). Stable 2σ-flow. Domains II, IV. (*c*) Velocity field (velocity vectors). Unstable σ-flow. Domains I, II. (*d*) Difference between 2σ-flow and σ-flow. Velocity field (velocity vectors). Domain II.

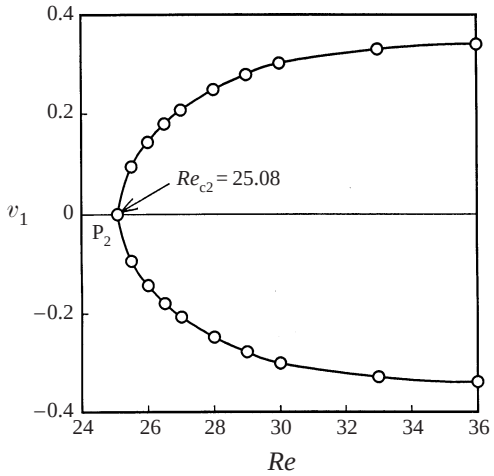

FIGURE 4. Representative velocity v_1, the velocity in the y-direction at $(x, y) = (1.5, \sigma/2)$, in the steady state: 2σ-flow, $\sigma = 1.7$. P_2: Pitchfork bifurcation point from σ-flow to 2σ-flow.

can easily imagine by a consideration of the symmetry that there is another solution obtained by shifting the flow field in figure 3(*a*) by σ in the y-direction, where the twin vortices attached to the bars at the top and bottom are smaller than those attached to the middle bar. There is one more steady solution, depicted in figure 3(*c*), which is unstable and calculated in domains I and III. Thus, we have found three steady solutions, i.e. two 2σ-flows and σ-flow, at $Re = 26$.

We can expect that some bifurcation of the steady solution happens between $Re = 24$ and 26, which was clarified as a symmetry-breaking pitchfork bifurcation by MT. In order to confirm the bifurcation, we take the velocities v_1, v_2, v_3, v_4 in the y-direction at $(x, y) = (1.5, \sigma/2)$, $(1.5, 3\sigma/2)$, $(1.5, 5\sigma/2)$, $(1.5, 7\sigma/2)$ as representative quantities which manifest the magnitude of asymmetry of the flow field (figure 1). There are relations $v_1 = -v_2 = v_3 = -v_4$ for 2σ-flow, whereas $v_1 = v_2 = v_3 = v_4 \equiv 0$ for σ-flow. The value of v_1 is plotted against Re in figure 4. We can confirm the relation $v_1 \propto (Re - Re_{c2})^{1/2}$, where Re_{c2} is the critical Reynolds number at which two 2σ-flows appear. The value of Re_{c2} is evaluated as $Re_{c2} = 25.08$ by applying the least-square method to the numerical data. Thus, we can reconfirm that the confluence of two jets occurs due to the pitchfork bifurcation, since the relation $v_1 \propto (Re - Re_{c2})^{1/2}$ holds. In other words, only σ-flow exists for $Re < Re_{c2}$, and two other solutions, 2σ-flows, appear at $Re = Re_{c2}$. The 2σ-flows are stable to disturbances with the period σ and σ-flow is unstable to disturbance with the period 2σ for $Re > Re_{c2}$.

We will call the difference between the stable 2σ-flow and the unstable σ-flow a disturbance. The velocity field of the disturbance is obtained by subtracting the velocity of σ-flow from that of 2σ-flow at each mesh point, which is shown in figure 3(*d*). Needless to say the disturbance has a periodicity of 2σ in the y-direction and a symmetry along the line $y = \sigma$. The disturbance is seen to consist of two large vortices whose centres are located on centrelines of the gaps between bars and about 2 times the side length downstream from the row of bars. It is also noted that the velocity of the disturbance is directed downstream behind the middle bar, and upstream behind the top and bottom bars in figure 3(*d*).

We will try to explain the physical process of the confluence of two jets. The pressure just behind the array of bars is low at the centres of jets and wakes in σ-flow

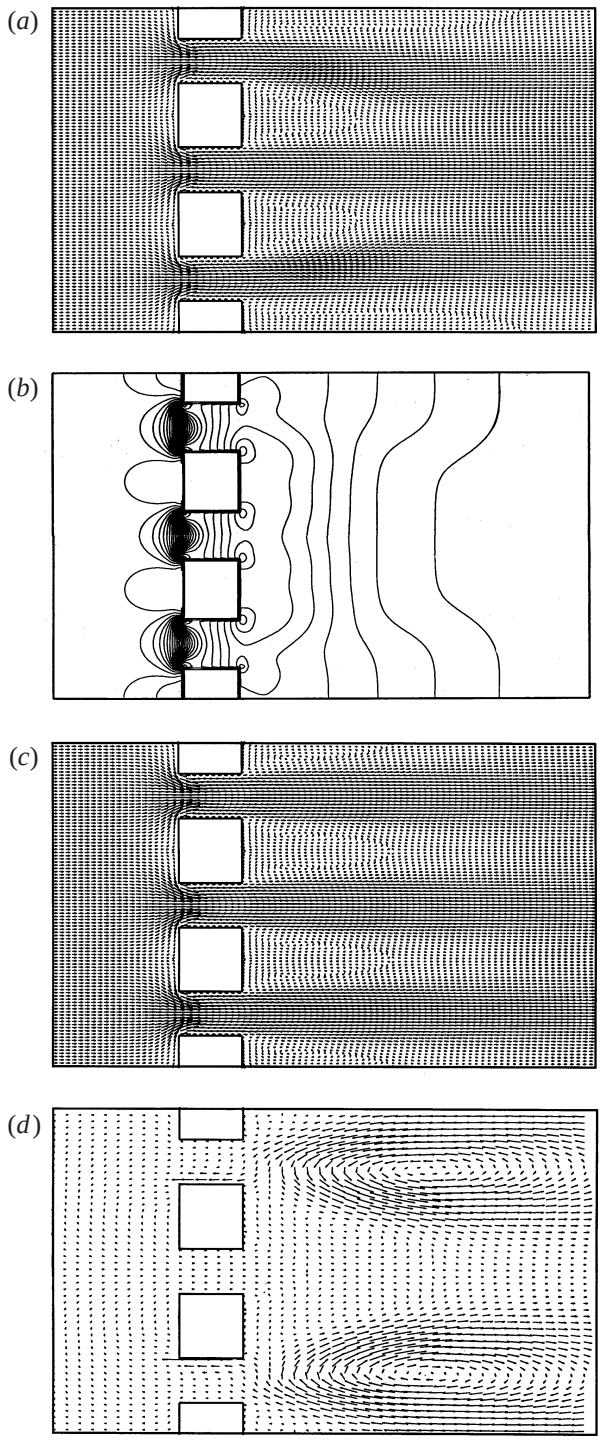

FIGURE 5. Flow fields. $Re = 27.5$, $\sigma = 1.7$. (*a*) Velocity field (velocity vectors). Stable 3σ-flow. Domain III. (*b*) Pressure (isobars). Stable 3σ-flow. Domain III. (*c*) Velocity field. Unstable σ-flow. Domain I. (*d*) Difference between 3σ-flow and σ-flow. Velocity field (velocity vectors). Domain III.

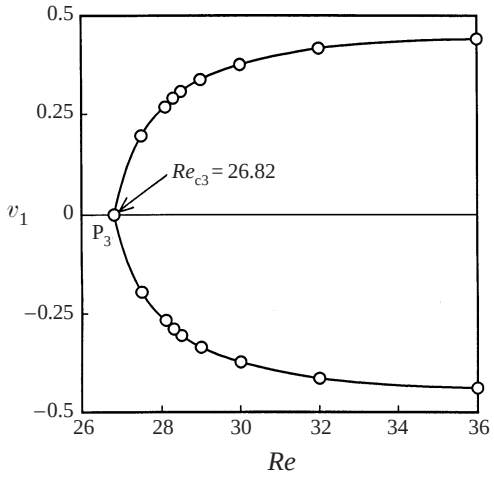

FIGURE 6. Representative velocity v_1, the velocity in the y-direction at $(x, y) = (1.5, \sigma/2)$, in the steady state. 3σ-flow. $\sigma = 1.7$.

as seen in figure 2(b) and the jets pull on each other. A jet is pulled from both sides and the tug is balanced when the Reynolds number is small. The jet bends to neither side due to a resistive force by the viscosity even if there is a small imbalance in the tug, but the balance is broken by a small disturbance at $Re = Re_{c2}$. The pressure just behind the array of bars is low only at the centres of every other wake in 2σ-flow as seen from figure 3(b). Thus the phenomenon is similar to the buckling of an elastic body.

We can obtain σ-flow in domain I and two 2σ-flows in domain II and IV at $Re = 27.5$ similarly to the case of $Re = 26$. However, the flow pattern changes in domain III when the Reynolds number is raised from $Re = 26$ to 27.5. The 3σ-flow appears in domain III at $Re = 27.5$, which is depicted in figure 5(a). The twin vortices attached to the bars are seen to change their sizes in sets of three in figure 5(a). Three jets coming through gaps between bars join into one behind the row of bars, the middle jet going straight. The corresponding pressure field is shown in figure 5(b). It is seen that contour lines of pressure which stem from the surfaces of the top and bottom bars are connected with each other in figure 5(b).

We explore the bifurcation point of 3σ-flow by taking the velocity v_1 in a similar manner to the case of 2σ-flow. It is noted here that $v_1 = -v_3 = v_4$ for 3σ-flow, while $v_2 \equiv 0$. So the velocity v_1 manifests the magnitude of the asymmetry of the flow field along the line $y = \sigma/2$. The value of v_1 is plotted against Re in figure 6. We can confirm the relation $v_1 \propto (Re - Re_{c3})^{1/2}$, where Re_{c3} is the critical Reynolds number at which two 3σ-flows appear. The value of Re_{c3} is evaluated as $Re_{c3} = 26.82$. Thus, we can reconfirm that the confluence of three jets occurs due to the pitchfork bifurcation from the σ-flow. We have seen that there are σ-flow, two 2σ-flows and two 3σ-flows for $Re > Re_{c3}$. The σ-flow is unstable to disturbances with the period 2σ or 3σ for $Re > Re_{c3}$, while the stabilities of 2σ- and 3σ-flows are not studied here.

The flow field of the unstable σ-flow at $Re = 27.5$ is shown in figure 5(c), where all the twin vortices attached to bars have an equal length. The disturbance defined by the difference between the stable 3σ-flow and the unstable σ-flow is depicted in figure 5(d). The flow pattern of the disturbance for 3σ-flow resembles to the one for 2σ-flow as shown in figures 5(d) and 3(d). In figure 5(d), we can see two larger vortices, whose

Re	v_1	v_2	$(v_1+v_2)^2$
30.0	0.088	−0.443	0.126
29.0	0.106	−0.409	0.091
28.5	0.125	−0.379	0.064
28.0	0.168	−0.320	0.023
27.7	0.233	−0.236	0.000

TABLE 2. Velocities v_1 and v_2 as the representative magnitude of the asymmetry of the bifurcated solution. $\sigma = 1.7$.

centres are located on centrelines of the gaps between bars and about 2 times the side length downstream from the row of bars. The velocity of the disturbance is directed downstream behind the two middle bars, and upstream behind the top and bottom bars.

The 4σ-flow is obtained as a steady solution in domain IV at $Re = 30$ as shown in figure 7(*a*). We can see four jets combining in this figure. The lengths of the twin vortices attached to bars vary in sets of four in the manner long, short, medium, short twin vortices and so on. The corresponding pressure field is depicted in figure 7(*b*). The contour lines of pressure which stem from the surfaces of the top and bottom bars are connected with each other, which reflects the mutual interaction between the four jets.

We have tried to find some relations of v_1, v_2, v_3 or v_4 to Re in order to explore the bifurcation point of 4σ-flow, but could not find any definite relations. Symmetry considerations lead to $v_1 = -v_4$ and $v_2 = -v_3$ for 4σ-flow, whereas $v_1 = -v_2 = v_3 = -v_4$ hold for 2σ-flow. So, the sum $v_1 + v_2$ manifests the magnitude of the difference between 4σ- and 2σ-flows, which is plotted against Re in figure 8 and tabulated in table 2. The relation $(v_1+v_2) \propto (Re-Re_{c4})^{1/2}$ holds near the critical point where Re_{c4} is the critical Reynolds number at which the 4σ-flow bifurcates from 2σ-flow. Thus we can conclude that the confluence of four jets is also due to pitchfork bifurcation. However, this bifurcation occurs from 2σ-flow at the critical Reynolds number Re_{c4}, which is evaluated as $Re_{c4} = 27.71$.

We can calculate an unstable solution of 2σ-flow for $Re = 30$ in domain II, which is shown in figure 7(*c*). The disturbance, which is defined as the difference between 4σ-flow and 2σ-flow, is depicted in figure 7(*d*). Four large vortices are observed in the figure, where each pair of adjacent vortices have the same sense of circulation.

We summarize the flow patterns obtained as steady solutions in domains I–IV for $\sigma = 1.7$ in figure 9. The global bifurcation diagram is easily imagined from this figure, but will be discussed in detail in § 3.3.

3.2. *Lengths of the twin vortices attached to the bars*

We can observe the bifurcations of steady solutions also from the change of lengths of the twin vortices attached to the bars in place of v_1 or $v_1 + v_2$. The lengths of the twin vortices l are plotted against Re in figures 10(*a*) and 10(*b*) for $\sigma = 1.7$ and are tabulated in table 3. In figure 10(*a*), we can see the dependence of l on the Reynolds number Re for σ-, 2σ- and 4σ-flows. The length l_1 of the twin vortices for σ-flow is shown by the line l_1 in figure 10(*a*). All the lengths are equal to each other for $Re < Re_{c2} = 25.08$ as seen in figure 10(*a*). The magnitude of l_1 increases almost linearly with the increase of Re.

At $Re = Re_{c2}$, the line l_1 splits into three, which are indicated as l_{2L}, l_1 and l_{2S}

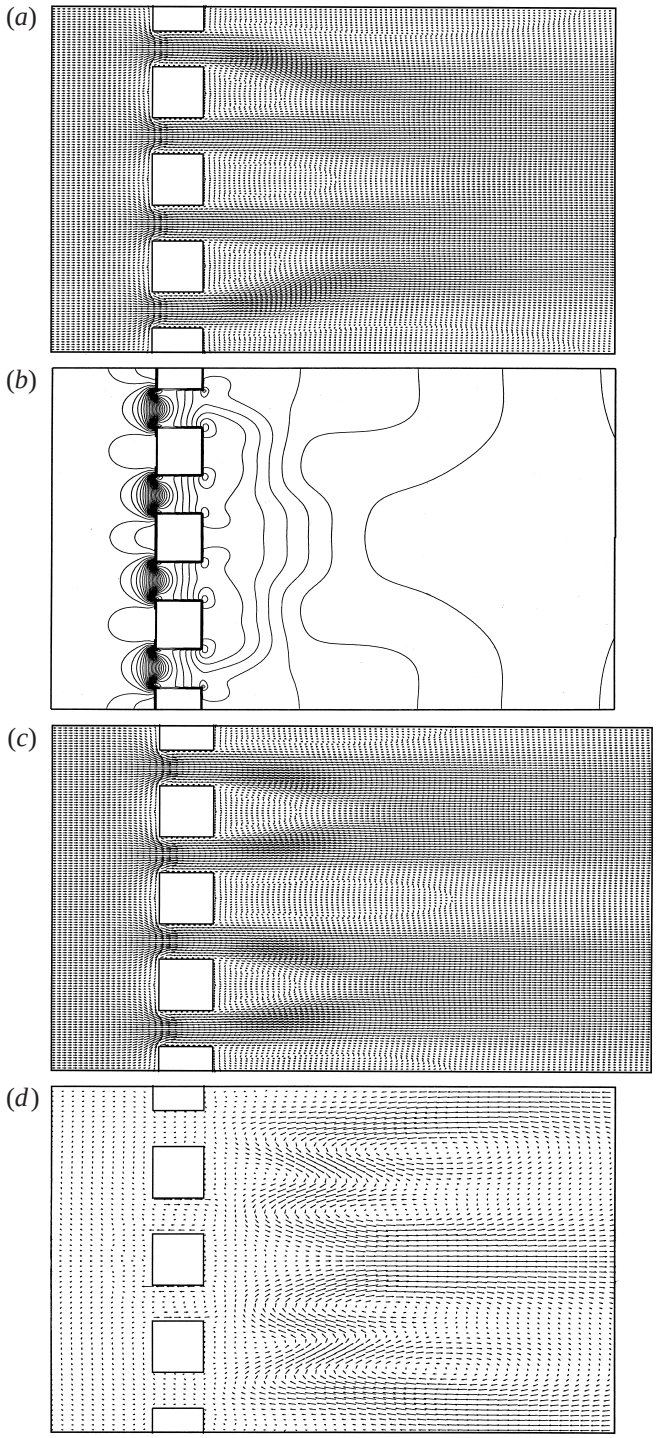

FIGURE 7. Flow fields. $Re = 30.0$, $\sigma = 1.7$. (*a*) Velocity field (velocity vectors). Stable 4σ-flow. Domain IV. (*b*) Pressure (isobars). Stable 4σ-flow. Domain IV. (*c*) Velocity field (velocity vectors). Unstable 2σ-flow. Domain II. (*d*) Difference between 4σ-flow and 2σ-flow. Velocity field (velocity vectors). Domain IV.

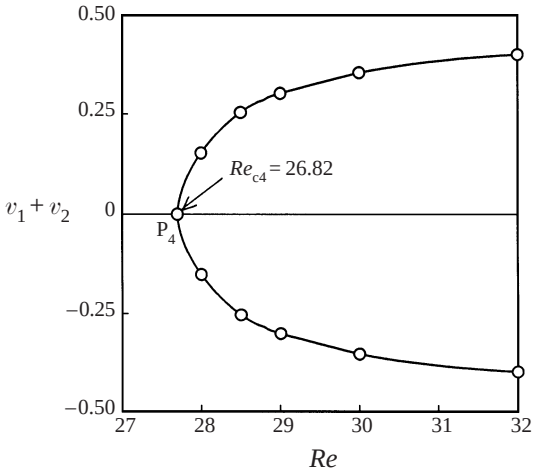

FIGURE 8. Representative velocity $v_1 + v_2$. 4σ-flow. P_4: Pitchfork bifurcation point from 2σ-flow to 4σ-flow. $\sigma = 1.7$.

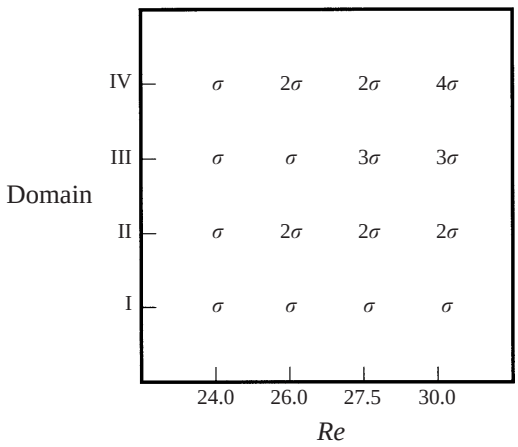

FIGURE 9. Summary of flow patterns obtained numerically in each computational domain. For instance, 4σ-flow is obtained as a steady-state solution by numerical calculations in numerical domain IV at $Re = 30$.

respectively. This splitting means that every other vortex become larger and the others smaller alternately as the Reynolds number becomes larger than Re_{c2}. So, the appearance of 2σ-flow corresponds to the alternate stretching and shrinking of twin vortices.

At $Re = Re_{c4}$, the line l_{2L} splits into three lines, which are indicated as l_{4L}, l_{2L} and l_{4M} respectively. In other words, half the larger vortices become still larger and the other half become smaller as the Reynolds number is raised above Re_{c4}, while smaller vortices with the length l_{2S} do not change their scale significantly.

In figure 10(*b*), the line l_1 for σ-flow splits into three lines, which are indicated as l_{3L}, l_1 and l_{3S} respectively. This splitting means that one in three of the twin vortices becomes larger, another becomes smaller and the third remains unchanged as the Reynolds number becomes larger than Re_{c3}. In this case, one of the twin vortices in every three stretches as seen in figure 5(*a*).

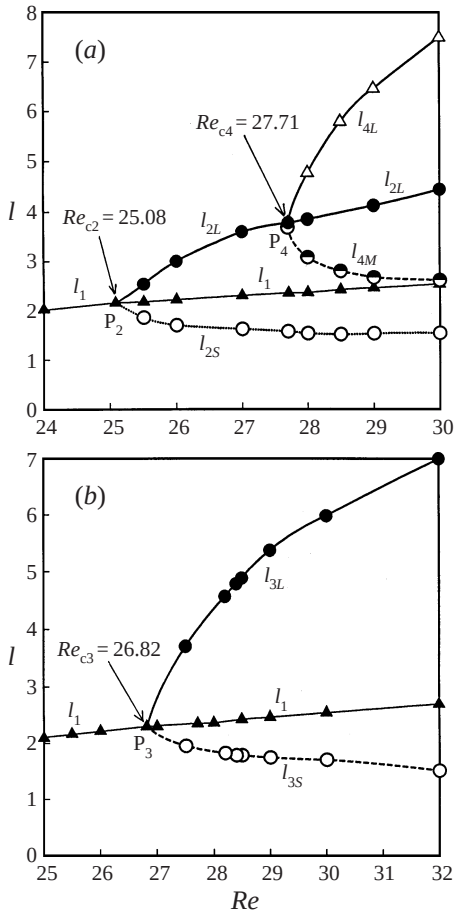

FIGURE 10. Lengths of the twin vortices l. $\sigma = 1.7$. (*a*) Domains I, II, IV. Filled triangles: l_1, filled circles: l_{2L}, open circles: l_{2S}, open triangles: l_{4L}, half-filled circles: l_{4M}. P_2: Pitchfork bifurcation point from σ-flow to 2σ-flow. P_4: Pitchfork bifurcation point from 2σ-flow to 4σ-flow. (*b*) Domains I, IV. Filled triangles: l_1, filled circles: l_{3L}, open circles: l_{3S}. P_3: Pitchfork bifurcation point from σ-flow to 3σ-flow.

3.3. *Bifurcation diagram*

The bifurcation diagram of the steady solutions is shown for $\sigma = 1.7$ in figure 11, where the representative velocity v_1 is plotted against Re. The horizontal line $v_1 = 0$ shows σ-flow, the other lines, indicate 2σ-, 3σ- and 4σ-flows. For $Re < Re_{c2}$, v_1 is identically zero, which shows that σ-flow is the only steady solution. At $Re = Re_{c2}$ a pitchfork bifurcation occurs and two solutions of 2σ-flow appear, whereas the σ-flow becomes unstable. The second bifurcation occurs at Re_{c4} and two branches of steady solution of 4σ-flow appear from each 2σ-flow. The 3σ-flows appear as a consequence of another pitchfork bifurcation at $Re = Re_{c3}$.

We have not studied the stability of the flows, but some information on their stability is obtained from figure 11. For instance, 2σ-flows are stable to disturbances with the periods σ and 4σ at $Re = 26$. The bifurcation diagrams for other values of σ are similar to figure 11.

	σ-flow	2σ-flow		3σ-flow		4σ-flow	
Re	l_1	l_{2L}	l_{2S}	l_{3L}	l_{3S}	l_{4L}	l_{4M}
24.0	2.03	—	—	—	—	—	—
25.0	2.13	—	—	—	—	—	—
25.5	2.17	2.65	2.65	—	—	—	—
26.0	2.22	—	—	—	—	—	—
26.5	—	2.98	1.74	—	—	—	—
27.0	2.29	—	—	—	—	—	—
27.5	—	3.24	1.66	3.70	1.95	—	—
27.7	2.35	3.46	1.62	—	—	—	—
28.0	2.36	3.80	1.56	—	—	4.76	3.08
28.5	2.42	—	—	4.88	1.78	5.78	2.92
29.0	2.45	4.12	1.56	5.37	1.74	6.45	2.67
30.0	2.54	4.44	1.56	5.98	1.70	7.49	2.62
32.0	2.72	—	—	7.00	1.51	—	—

TABLE 3. Length l of the twin vortices attached to the square bars. $\sigma = 1.7$.

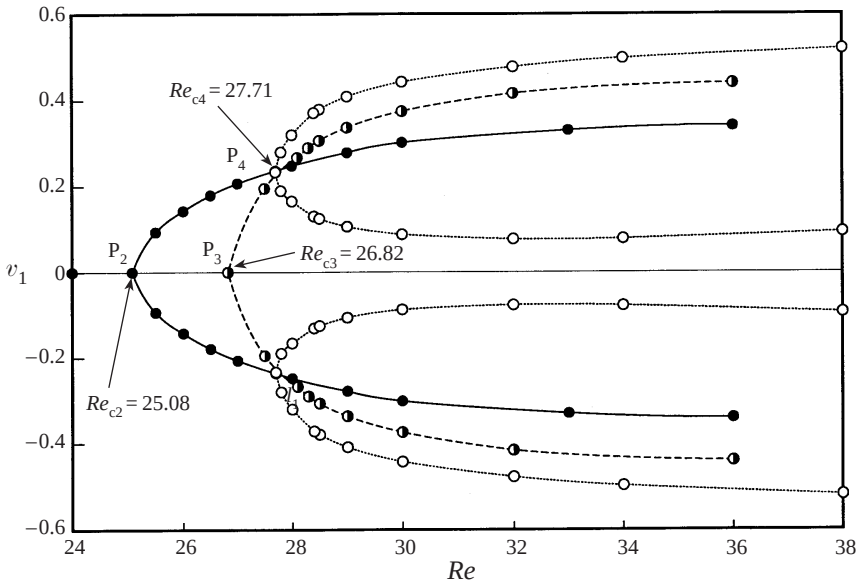

FIGURE 11. Global bifurcation diagram. $\sigma = 1.7$. Filled circles: 2σ-flow, half-filled circles: 3σ-flow, open circles: 4σ-flow. P_2: Pitchfork bifurcation point from σ-flow to 2σ-flow. P_3: Pitchfork bifurcation point from σ-flow to 3σ-flow. P_4: Pitchfork bifurcation point from 2σ-flow to 4σ-flow.

3.4. *Critical Reynolds numbers*

We have done similar numerical simulations for $\sigma = 1.4$, 1.5 and 1.6 as well as $\sigma = 1.7$ and evaluated the critical Reynolds numbers Re_{c2}, Re_{c3} and Re_{c4} for each aspect ratio σ. The critical Reynolds numbers Re_{c2}, Re_{c3} and Re_{c4} are shown in figure 12 and are tabulated in table 4. In figure 12, only σ-flow is the steady solution in the region under the line indicated by Re_{c2}. In the region between the two lines indicated by Re_{c2} and Re_{c3}, 2σ-flow is also a steady solution as well as unstable σ-flow. The 3σ- and 2σ-flows are steady solutions as well as unstable σ-flow in the region between the two lines indicated by Re_{c3} and Re_{c4}. It cannot be predicted which flow, 2σ or

	Re_{c2}		Re_{c3}		
σ	Present result	MT	Present result	MT	Re_{c4}
1.4	19.27	—	20.94	—	21.47
1.5	20.96	—	22.64	—	23.54
1.6	22.00	23.16	23.90	24.65	25.60
1.7	23.20	25.08	26.40	26.82	27.71

TABLE 4. Critical Reynolds numbers Re_{c2}, Re_{c3} and Re_{c4}. Re_{c2} is the critical Reynolds number for the bitchfork bifurcation from σ-flow to 2σ-flow, Re_{c3} from σ-flow to 3σ-flow and Re_{c4} from 2σ-flow to 4σ-flow.

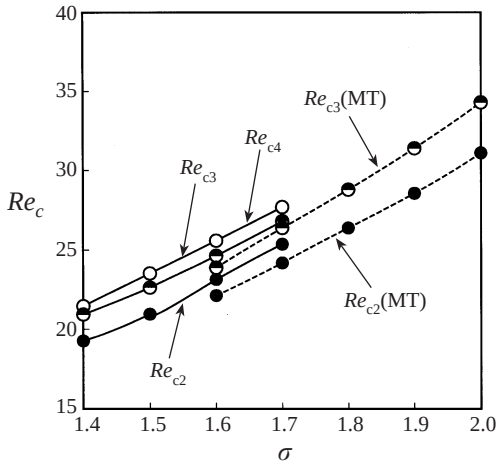

FIGURE 12. Critical Reynolds numbers. Solid line with filled circles: Re_{c2} (present result), solid line with half-filled circles: Re_{c3} (present result), solid line with open circles: Re_{c4}(present result), dotted line with filled circles: Re_{c2} (MT), dotted line with half-filled circles: Re_{c3} (MT).

3σ, may appear in this range because the stability of the flows is not studied in this paper. The critical values Re_{c2} and Re_{c3} obtained by MT are shown for comparison. Our critical values of Re_{c2} and Re_{c3} are 7.5% smaller than those by MT at most. The difference may come from the insufficient resolution of computational region used by MT. However, any direct comparisons of mesh sizes are not possible because they used a non-equally distributed mesh whereas we used an equally distributed mesh.

We have evaluated the critical Reynolds numbers for the appearance of the combination phenomena of two, three, four jets for a fixed value of σ, but most experiments so far have been done to seek the critical aspect ratio σ_c for a fixed value of Re. Such a critical aspect ratio σ_c can be found from figure 12. For instance, the critical aspect ratio σ_{c2} for the occurrence of the combining of two jets at Re_1 is given by the intersection of the line indicated by Re_{c2} and a line of $Re = Re_1$.

4. Experimental method and results

We did experiments to obtain flow visualizations. The experiments were done in a suction-type wind tunnel which has a test section $225 \times 225\,\mathrm{mm}^2$ in cross-section and 1000 mm in length. The kinematic viscosity ν of air was $0.015\,\mathrm{cm}^2\,\mathrm{s}^{-1}$ at the temperature in our laboratory. It was confirmed that the tunnel provides an almost

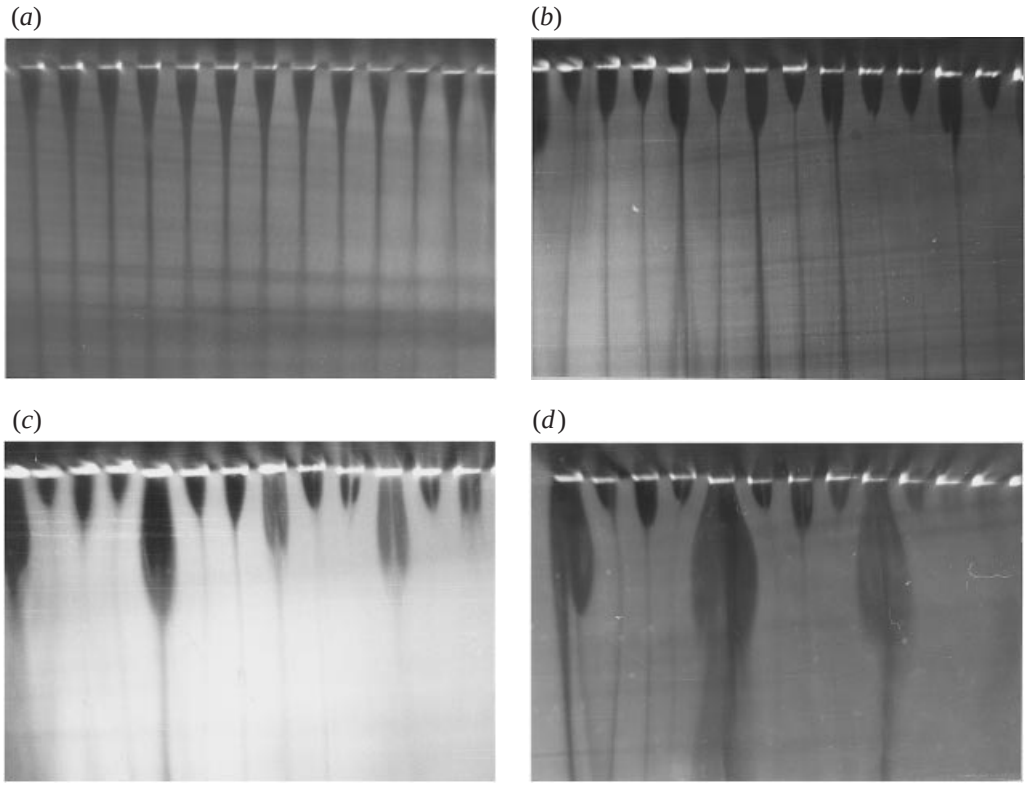

FIGURE 13. Typical flow patterns visualized by smoke from dry ice. $\sigma = 1.7$. Flow direction is from the top to the bottom. (*a*) σ-flow. $Re = 25$. (*b*) 2σ-flow. $Re = 28$. (*c*) 3σ-flow. $Re = 34$. (*d*) 4σ-flow. $Re = 40$.

uniform flow except for the wall boundary layers. The uniform velocity ranges from $130\,\mathrm{mm\,s^{-1}}$ to $1100\,\mathrm{mm\,s^{-1}}$. A row of square bars with the side length $d = 4\,\mathrm{mm}$ was set parallel to the side of the test section. The distance P between the centre of adjacent square bars is fixed as $P = 6.8\,\mathrm{mm}$ so that the corresponding pitch-to-side-length ratio σ is 1.7.

For the visualization of the flow, smoke from dry ice was used. A sheet of light from a slide projector is thrown on the test section at its mid-height to take pictures of the flow. The uniform velocity U was measured at the centre of the entrance of the test section by a hot wire, which was adopted as a representative velocity in the definition of $Re \equiv Ud/\nu$.

It is stressed here that we do not intend to obtain the bifurcation diagram of the flow nor to determine the critical Reynolds number by the experiments, but we aim to realize steady confluent flows experimentally and visualize them. So the uniform velocity, i.e. the Reynolds number, is not increased quasi-statically in our experiments, but is changed to-and-fro to seek steady confluent flow patterns.

The flow patterns thus obtained are depicted in figures 13(*a*)–13(*d*) for $Re = 25, 28, 34, 40$ respectively. In each figure, the flow direction is from the top to the bottom, and streak lines are visualized as lighter broad lines that are brightened by the reflected light from the dry ice smoke. The dark regions roughly correspond to twin vortices attached to the bars. In figure 13(*a*) for $Re = 25$, the lengths of the twin vortices attached to the square bars are almost the same as each other. The lengths are

roughly measured from the figure as $l_1 = 2.3d$–$2.72d$, which should be compared to the numerical result of $l_1 = 2.13$. The difference between the experimental and numerical results is rather small. The jets are almost parallel to the uniform flow upstream and the flow field has a periodicity of σ in the direction normal to the stream. Figure 13(b) shows the flow field for $Re = 28$. The lengths of twin vortices vary alternately and the flow field has a periodicity of 2σ in the direction normal to the stream although a confluence of four jets is also seen in the left-hand side of this figure. The lengths are measured from the figure as $l_{2S} = 1.6d$–$2.0d$ and $l_{2L} = 2.6d$–$2.9d$, which should be compared to the numerical results of $l_{2S} = 1.56d$ and $l_{2L} = 3.80$. The experimental and numerical results for l_{2L} differ significantly although the lengths l_{2S} coincide with each other. It is thought that the difference may come from a slight non-uniformity of the uniform flow in the wind channel. The visualized streaklines extend straight downstream in figure 13(b). This suggests that the flow is almost steady. The critical Reynolds number Re_{c2} for the appearance of 2σ-flow is expected between $Re = 25$ and 28. The combining of three jets (3σ-flow) is seen in figure 13(c) for $Re = 34$ although the periodicity 3σ is not very clear. We can see the flow field with the period of 4σ in figure 13(d) for $Re = 40$. It is clearly seen that the combining of four jets occurs by the coalescences of pairs of two combined jets in the figure.

It is reconfirmed that the confluence of jets occurs and the flow pattern changes as the Reynolds number is increased for a fixed value of σ, i.e. $\sigma = 1.7$. This is in contrast to almost all experiments (Bohl 1940; Bradshaw 1965; Moretti & Chen 1987; Moretti 1993) which have been done so far, which were in order to explore the critical pitch-to-side-length ratio σ_c for a given value of the Reynolds number.

5. Conclusions

It is our conclusion that 4σ-flows appear as a result of the second pitchfork bifurcation from the bifurcated 2σ-flow, whereas 2σ- and 3σ-flows arise due to the first pitchfork bifurcation from σ-flow. So, the present result is not only an extension of the number of jets but also an extension of the stage of transitions compared to previous work.

We have attempted a physical explanation for the confluence phenomena in § 3.1, but it may not seem very convincing. It is expected that a more convincing explanation will be given for the phenomena.

It is found that 4σ-flow appears as a result of instability of 2σ-flow. This reminds us of period-doubling bifurcations, although the spatial period is considered in the present case in place of the usual time period. It is our speculation that there may be a spatial period-doubling bifurcation in the flow past a row of square bars. On the other hand, it is expected that two other solution branches of 4σ-flow may bifurcate directly from σ-flow at very high Reynolds number. However, the branches have no physical significance because the σ-flow is unstable at such high Reynolds numbers and the 4σ-flows are not easily realized in experiments.

We have not studied the stability of the flows. MT pointed out that there is a discrepancy between the critical Reynolds numbers Re_{c3} obtained by experiments and numerical simulations, although the values of Re_{c2} evaluated experimentally and numerically coincide. They conjectured that this discrepancy may come from a hysteresis phenomenon, which appears when experiments or simulations are done by increasing or decreasing the Reynolds number. Our experiments were conducted just to realize the confluent steady flows, so the discrepancy was not resolved. Precise experiments and stability analyses of the steady solutions are expected to resolve the

discrepancy between experiments and numerical results and to confirm the hysteresis conjectured by MT.

As for flows past a single square bar, a Hopf bifurcation occurs as the first bifurcation. The flow is steady and symmetric for $Re < Re_c$. The symmetric flow becomes unstable at Re_c and time-periodic flows appear due to the instability. The critical Reynolds number Re_c is evaluated as $Re_c = 48.8$ by MT. The critical Reynolds number for the flow past a circular cylinder was evaluated as $Re_c = 46.2$ by Jackson (1987). The flow past a circular cylinder was shown to be almost two-dimensional for $Re \leqslant 180$.

We have confined ourselves to steady flows in the present paper, so only pitchfork bifurcations are found. However, if we extend our numerical simulations to unsteady flows, Hopf bifurcations are expected to lead to the confluence of several jets occurring in time-periodic flows where vortices detached from bars make a periodic pattern in the transverse direction to the flow with twice the period of the bars at moderate Reynolds numbers ($Re \sim 210$) (Kobayashi, 1984) and turbulent flows ($Re \sim 3000$) (Matsui, 1975).

The authors express their cordial thanks to Professors T. Matsui, H. Yamaguchi, S. Narita and Dr T. Adachi for valuable discussion. This work was partially supported by a Grant-in-Aid from the Ministry of Education, Science and Culture and also by Doshisha University's Research Promotion Funds.

REFERENCES

Beaumont, D. N. 1981 The stability of spatially periodic flows. *J. Fluid Mech.* **108**, 461–474.

Bohl, J. G. von 1940 Das Verhalten paralleler Luftstrahlen. *Ing.-Arch.* **11**, 295–314.

Bradshaw, P. 1965 The effect of wind-tunnel screens on nominally two-dimensional boundary layers. *J. Fluid Mech.* **22**, 769–687.

Gotoh, K., Yamada, M. & Mizushima, J. 1983 The theory of stability of spatially periodic parallel flows. *J. Fluid Mech.* **127**, 45–58.

Green, J. S. A. 1974 Two-dimensional turbulence near the viscous limit. *J. Fluid Mech.* **62**, 273–287.

Jackson, C. P. 1987 A finite-element study of the onset of vortex shedding in flow past variously shaped bodies. *J. Fluid Mech.* **182**, 23–45.

Kobayashi, T. 1984 In *Shashinshu Nagare* (*Collected Photographs of fluid flows*) (ed. Japan Soc. Mech. Eng.), p. 43. Maruzen (in Japanese).

Matsui, T. 1975 Cross flow through a row of heated rods. *Proc. 1975 Joint JSME-ASME Applied Mechanics Western Conference, Honolulu, Hawaii*, pp. 415–421. Japan Soc. Mech. Engrs.

Mizushima, J. & Takemoto, Y. 1996 Stability of the flow past a row of square bars. *J. Phys. Soc. Japan* **65**, 1673–1685 (referred to herein as MT).

Moretti, P. M. 1993 Flow-induced vibrations in arrays of cylinders. *Ann. Rev. Fluid Mech.* **25**, 99–114.

Moretti, P. M. & Chen, M. 1987 Instability of flow through tube rows. *Trans. ASME: J. Fluid Engng* **109**, 197–198.

Yamada, M. 1986 Nonlinear stability theory of spatially periodic parallel flows. *J. Phys. Soc. Japan* **55**, 3073–3079.